Patterns in inhibitory networks of simple map neurons

Borja Ibarz,[1] José Manuel Casado,[2] and Miguel A. F. Sanjuán[1]

[1]*Nonlinear Dynamics and Chaos Group, Departamento de Física, Universidad Rey Juan Carlos, Tulipán s/n, 28933 Móstoles, Madrid, Spain*

[2]*Area de Física Teórica, Universidad de Sevilla, 41080 Sevilla, Spain*

We study the dynamics of networks of inhibitory map-based bursting neurons. Linear analysis allows us to understand how the patterns of bursting are determined by network topology and how they depend on the strength of synaptic connections, when inhibition is balanced. Two kinds of patterns are found depending on the symmetry of the network: slow cyclic patterns riding on subthreshold oscillations where almost all neurons contribute bursts in a sparse manner and fast patterns of bursts in which only one of two mutually exclusive groups of neurons take part. We also discuss the properties of the neuron model that underlie the described phenomena, comment on the limitations of the technique of analysis, and point to some possible ways to overcome them.

I. INTRODUCTION

The behavior of networks of coupled neurons is a central topic in theoretical neuroscience [1]. In these complex systems, collective synchronous activity seems to be critical to the efficient processing of information by the nervous system. In the past decade a great deal of theoretical and experimental work has been done to analyze synchronizing behavior in a great variety of ensembles of neurons and other excitable cells. Among these, some of the best studied are those made up by bursters; they include thalamic neurons during periods of sleep or drowsiness [2], dopaminergic neurons in the midbrain [3], pancreatic β cells [4], and central pattern generator neurons. Reciprocal inhibition is a core feature in most of these, and has been intensively studied as a pattern generating mechanism in rhythmic tasks such as swimming, walking, heartbeat, and respiration [5,6].

From the theoretical point of view, it is of great interest to understand how the structure of these inhibitory networks determines the observed patterns. Previous work by the authors has investigated this topic in the context of winnerless competition [7] and sensory encoding [8]. In the present contribution we establish the validity of linear analysis to predict complex patterns in networks of inhibitory bursting neurons, provided that certain conditions hold. One of the conditions is balance, which means that all neurons should receive the same amount of inhibition. As opposed to excitatory or diffusive connections, where the total number of signals received by each neuron is the only parameter that matters for synchronization [9], we shall see that the patterns formed due to balanced inhibitory synapses depend and may be predicted on the basis of higher order properties of the topology.

Network models supporting global or partial synchronized states have been generally formulated by describing each neuron by means of a set of differential equations linking the rate of change of the membrane potential to the temporal evolution of one or more gating variables that account for the intrinsic dynamics of the neuronal membrane. Thus, in order to simulate an ensemble of 10^3 neurons a few thousand coupled differential equations have to be simultaneously solved. For the purpose of simulating the behavior of large networks of neurons it is convenient to choose simpler models that, while retaining the features relevant to the phenomena under investigation, reduce the computational and analytical complexity of the problem as much as possible [10,11]. In the past few years another class of neuron model has been introduced in which the single neuron dynamics is represented by means of a two-dimensional map [12]. Recently, a model of this kind has been successfully used to describe the global behavior of large cortical networks, thus proving the feasibility of replicating prominent spike pattern characteristics of complex systems by using this computationally efficient approach [10]. Although we will not be dealing here with large networks, the model presents the additional particularity of a neutrally stable slow variable, which allows for easy tracking of its fixed point and enhances resonance properties [13]. Both features are convenient for the present investigation.

We begin with a description of the map-based neuron model of our choice and the connection scheme. We then proceed to describe some typical examples of patterns in small networks. The core of the paper lies in the section devoted to the stability analysis of fixed points; here the relationship between topology and patterns is clarified, the sensitivity of patterns to the strength of inhibition is explained, and a classification of the networks regarding their synchronization properties emerges. We then discuss some limitations of our investigation and hint at remedies and extensions.

II. NEURON MODEL

We consider the neuron map model proposed by Rulkov [14], which responds to equations

$$x_{n+1} = f(x_n, y_n + \beta),$$

$$y_{n+1} = y_n - \mu[x_n - \sigma + 1], \tag{1}$$

where
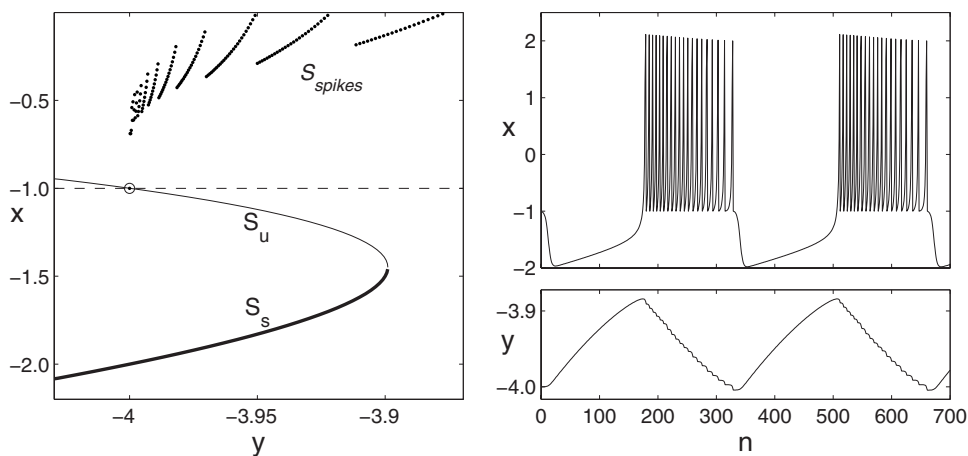
FIG. 1. Left: Bifurcation diagram for the Rulkov single-neuron fast subsystem. S_s and S_u are the stable and unstable branches of the fast dynamics, while S_{spikes} represent mean values of the fast variable x in the spiking cycle of each value of the slow variable y. The horizontal dashed line is the slow subsystem nullcline, at $x=-1+\sigma$. Right: Time evolution of the two variables of the Rulkov model. Parameters are $\alpha=6.0$, $\mu=0.001$, and $\sigma=0$.

$$f(x,y) = \begin{cases} \alpha(1-x)^{-1} + y, & x \leq 0 \\ \alpha + y, & 0 < x < \alpha + y, \\ -1, & x \geq \alpha + y. \end{cases} \quad (2)$$

In this model, μ is a small parameter, and therefore x_n is the fast variable, representing an appropriately scaled membrane voltage, whereas y_n is a slow gating variable. Parameter α defines the behavior of the neuron: $\alpha > 4$ allows bursting while $\alpha < 4$ does not. Two types of external excitations may enter this model: β directly pulls the fast variable toward higher values, and therefore is comparable to injected current, while σ enters the slow variable equation and has a modulatory effect. In the present work we will connect neurons through the slow variable.

Phase plane analysis through nullclines gives us very valuable insights about the behavior of the map [14]. Since $0 < \mu \ll 1$, the time course of y_n is much slower than that of x_n. Thus we can study the dynamics of the fast variable by treating y_n as a parameter in the first of Eqs. (1). In Fig. 1 the fast variable nullclines form a concave curve with two branches as a function of parameter y. The upper branch S_u corresponds to unstable fixed points of the fast subsystem and the lower branch S_s to its stable fixed points. The slow variable nullcline is a horizontal straight line (given by $x=-1+\sigma$); whenever the state is above (under) this line the slow variable y moves toward the left (right). If we now include the dynamics of the slow variable, we can understand the mechanism of bursting. When $\sigma=0$, as in the figure, the slow nullcline coincides with the $x=-1$ line where every trajectory that shoots above the unstable x nullcline returns after a spike. If this line intersects the unstable branch of the x nullcline (which happens only if $\alpha > 4$), the system is able to produce bursts. Dotted curves S_{spikes} represent average values of the fast variable x for each value of the variable y when the neuron is spiking.

The Rulkov map has one and only one fixed point at the intersection of the x and y nullclines. Changes in the stability of this fixed point take place through changes in σ and are due to a subcritical Neimark-Sacker bifurcation. For $\mu \ll 1$, this happens when the slow nullcline crosses the vertex of the fast nullcline, that is, when $-1+\sigma \approx 1 - \sqrt{\alpha}$.

An important feature of the model is the neutral, instead of exponential, stability of the slow variable, i.e., the fact that

it has no tendency to grow or shrink when perturbed. This translates into a horizontal slow nullcline in the phase plane. As a consequence, fast currents, embodied in the β term, have only transient effects on the dynamics, because they merely shift the fast nullcline horizontally, and thus leave the phase plane configuration intact [13]. It is for this reason that we will use instead slow coupling to observe the formation of patterns in our networks.

In order to form networks, we consider one of the simplest models of synapses between the neurons: A linear, thresholded injection of current [11]. This means that the interaction term is directly proportional to the presynaptic neuron voltage, as long as it is above a certain level. This does not mean that the corresponding synapses are fast, because the interaction will enter the slow variable. We are interested in the role of inhibition in pattern formation, so synapses will be inhibitory. The complete model for our neural network is

$$x_{n+1}^i = f(x_n^i, y_n^i),$$

$$y_{n+1}^i = y_n^i - \mu^i\left[x_n^i + 1 - \sigma^i - \sum_j g_c^{ij}(x_n^j - \phi^j)H(x_n^j - \phi^j)\right].$$

$$(3)$$

In these equations, index i runs from 1 to N, the total number of neurons. The synaptic strength of connection between neuron i and neuron j is given by $g_c^{ij} \leq 0$. $H(x)$ is the Heaviside step function and ϕ_j is the threshold value for the the variable x above which the presynaptic neuron j is supposed to influence postsynaptic neurons. This value is taken as $\phi=-2$ by default in our simulations; we will discuss the importance of this low threshold. Finally, σ^i is the constant external bias for each neuron. In what follows we will refer to homogeneous networks where all neurons share the same α, μ, σ, and ϕ parameters. In Sec. V we will discuss briefly the effect of inhomogeneity.

III. DYNAMICS IN NETWORKS WITH BALANCED INHIBITION

Networks with a high degree of symmetry, such as rings or lattices, are, because of their simplicity, usual choices for
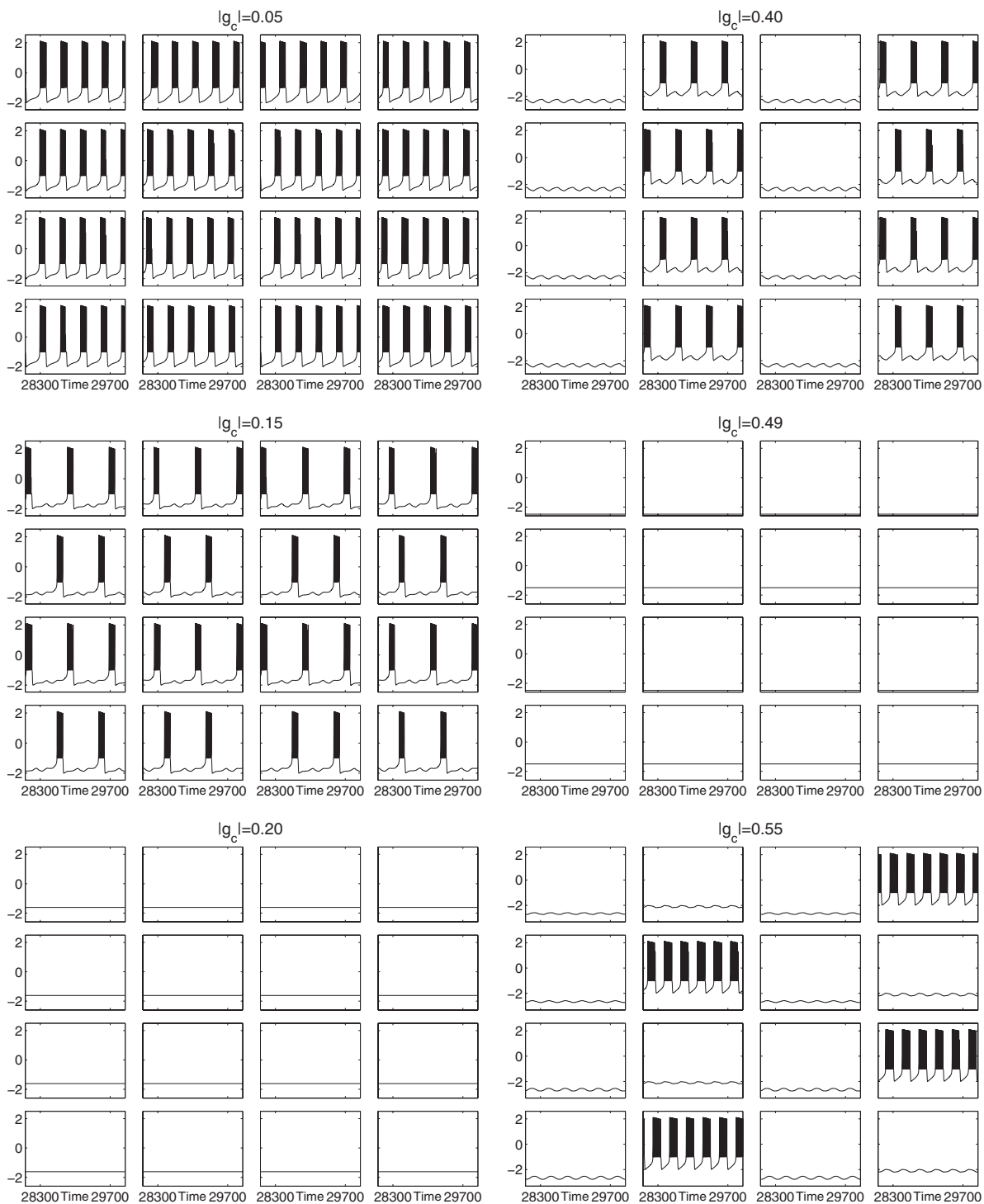
FIG. 2. Patterns of activity in a homogeneous 4×4 periodic two-dimensional lattice with eight nearest neighbors, for different values of g_c. Other parameters are $\alpha=6$, $\mu=0.001$, $\sigma=0$, and $\phi=-2$.

studies of network dynamics. We begin our investigation with a small 4×4 periodic two-dimensional lattice of Rulkov neurons with $\alpha=6$, $\mu=0.001$, and $\sigma=0$. This makes them, when isolated, periodic bursters. Each neuron will be connected to its eight nearest neighbors with a coupling strength g_c that we will use as a parameter to explore different behaviors of the network. The network is thus completely regular and symmetric. The only asymmetry that will enter

the following simulations is the initial state of each neuron, which will be chosen randomly to allow us to investigate the different attractors for each value of synaptic strength g_c.

Figure 2 represents the x variable of each neuron in our 4×4 lattice for different values of inhibitory strength $|g_c|$. When inhibition is weak, all neurons in the lattice fire, adopting different antiphase synchronization patterns (row or column for $g_c=-0.05$; checkered for $g_c=-0.15$). This has been

partially explained in a previous paper [11]. It is apparent
that the duty cycle of each neuron decreases with increasing
$|g_c|$, giving rise to the expected decrease in activity. Then
for $g_c = -0.20$ all neurons become silent; seemingly, inhibi-
tion is so strong that no single neuron can be active. When
activity reappears beginning at $g_c = -0.25$ (we show the case
$g_c = -0.40$), only half of the neurons are active. After a sec-
ond interval of silence ($g_c = -0.49$), activity reappears exclu-
sively in isolated neurons ($g_c = -0.55$) with a very long duty
cycle because now they have no inhibiting neighbors.

   All of the above is equally valid for any $2n \times 2m$ square
lattice with an eight-neighborhood: The same patterns appear
at the same values of inhibition. Other planar lattices (square
with 4-neighborhood; triangular, hexagonal, etc.) show dif-
ferent patterns, but they all share the same trend: For low
inhibition all neurons are active, then all become silent, then
some neurons regain activity while others remain silent, and
so forth.

   The network needs not have a high degree of symmetry
for the pattern formation phenomenon to appear. In Fig. 3 the
activity of a network based on a regular random graph of
$N=16$ vertices with degree $\nu=6$ (that is, six synapses per
neuron) is represented. Connections are bidirectional. For
weak values of inhibition (not shown in the figure) the all-
active ($g_c > -0.22$) and the all-silent ($-0.24 < g_c < -0.22$)
configurations are obtained, just as in the case of the lattice.
When inhibition is stronger (as in the figure, where
$g_c = -0.3$) some of the neurons fire. Two complementary
groups of neurons emerge and one or the other will be active
depending on the initial conditions. Note that the number of
synapses each neuron receives is the same and thus the ex-
planation of the pattern depends on higher order properties of
the network.

   Why do these networks become silent and what triggers
the reappearance of activity from total silence when inhibi-
tion increases further? The answer to the first part of this
question is straightforward: Increasing inhibition is equiva-
lent to decreasing σ in Eqs. (1). This brings the slow
nullcline in Fig. 1 down until it crosses the stable branch of
the fast nullcline and thus neurons draw each other into si-
lence. For this effect only the first order properties of the
network (that is, the degree) are important: The higher the
degree, the less strength of individual synapses will be
needed. But the loss of stability of this equilibrium with even
stronger inhibition is more complex: It requires small posi-
tive voltage perturbations in one neuron to cause negative
excursions in its neighbors that will in turn produce positive
changes in second order neighbors, and so on, in a way that
amplifies the original perturbation. That is, it depends on
network modes. The next section shows indeed how linear
analysis predicts the patterns in Figs. 2 and 3, and highlights
the features of the neuron model that make them possible.

IV. STABILITY ANALYSIS

   The networks we are going to study share the property of
balanced inhibition. This means that the weighted sum of
synapses arriving at each neuron is the same, or, in terms of
Eqs. (3), that the row sum $\Sigma_j g_c^{ij}$ is a constant independent of
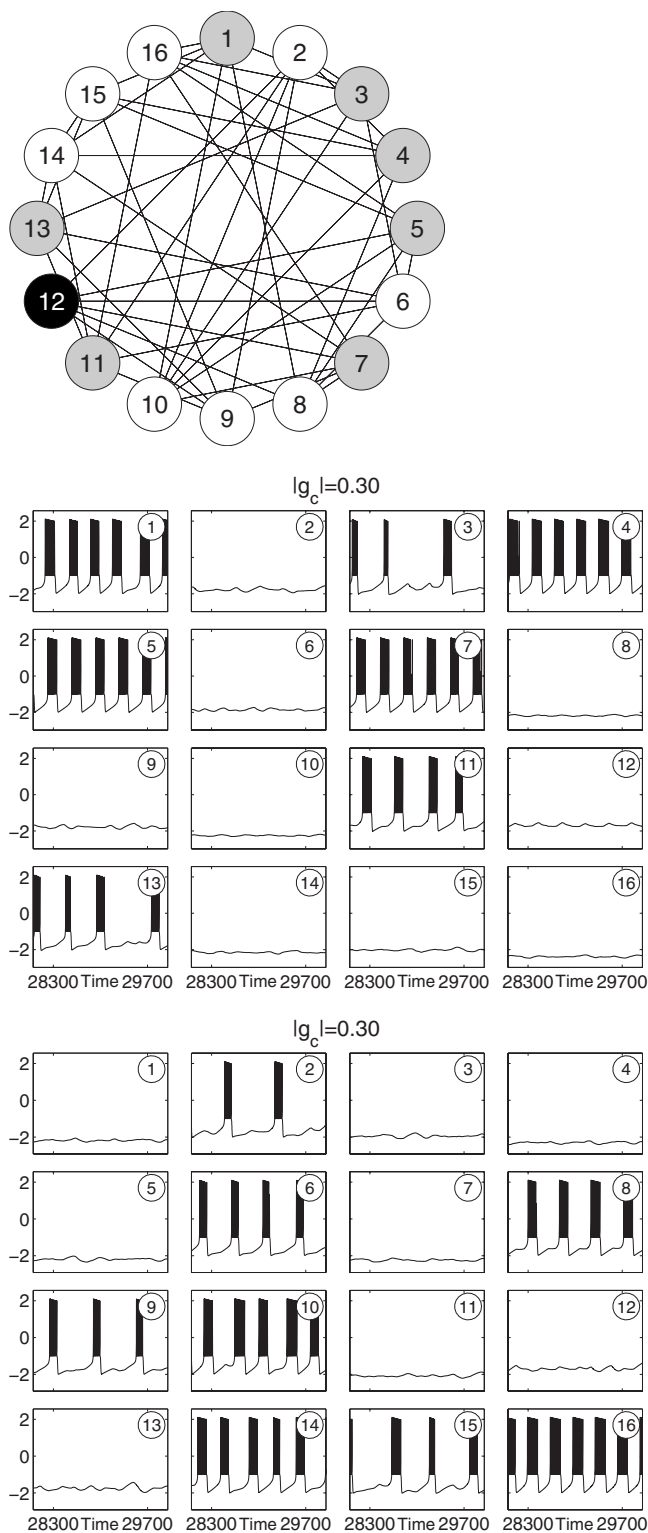
FIG. 3. Patterns of activity in a random regular network of $N
=16$ neurons with $\nu=6$ bidirectional connections. Top: The structure
of the network. White and gray neurons represent the two possible
groups of active neurons when inhibition is strong ($g_c < -0.25$).
Neuron 12 is inactive in all cases. Center and bottom: Two different
simulations of the network with $g_c = -0.3$ showing the two possible
groups of active neurons. Although graphically distributed as a lat-
tice, connection between the neurons is as on the top. Other param-
eters are $\alpha=6$, $\mu=0.001$, $\sigma=0$, and $\phi=-2$.

i. This is a generalization of the concept of a balanced network [15] where the row sums are 0; in our inhibitory networks, the constant row sum is negative. Symmetric networks based on regular graphs, such as those we have so far presented, are particular cases of networks with balanced inhibition, and we will refer to them as regular networks.

The balance property together with homogeneity in neuron parameters ensures that the synchronized state where $(x_n^i, y_n^i) = (x_n^j, y_n^j)$ for any i and j is an invariant manifold of the system. We now show that, with a low synaptic threshold ϕ, this manifold will contain a fixed point whose stability determines the disappearance of activity in the network and the rebirth of activity with stronger inhibition, as shown in Fig. 2. Indeed, in the general case the fixed points of Eqs. (3) must satisfy the following condition, given by the slow variable equation:

$$x_*^i = -1 + \sigma^i + \sum_j g_c^{ij}(x_*^j - \phi^j)H(x_*^j - \phi^j), \quad i = 1, \ldots, N.$$

(4)

The Heaviside function forbids a straightforward solution of this system, but its thresholding character allows a trial and error approach by postulating first which neurons are above or below the threshold. Thus for the equilibrium solution where all neuron voltages x_*^i are above the chemical interaction threshold ϕ^j, Eqs. (4) can be simply written as the linear system

$$\mathbf{x}_* = -\mathbf{1}_N + \sigma + g_c\Gamma_c(\mathbf{x}_* - \phi),$$

(5)

where $\mathbf{1}_N$ is the all-ones column vector of length N, $\mathbf{x}_* = (x_*^1, \ldots, x_*^N)^T$, $\sigma = (\sigma^1, \ldots, \sigma^N)^T$, and $\phi = (\phi^1, \ldots, \phi^N)^T$. We have introduced a common g_c as a convenient scaling parameter for the strength of the synapses; it will be negative for inhibition. Γ_c is the adjacency matrix of synaptic connections, with values $\gamma_c^{ij} = 1$ or $\gamma_c^{ij} = 0$ depending on whether or not there exists a synapse from neuron j to neuron i, and constant row sums $\nu = \Sigma_j \gamma_c^{ij}$ for our balanced networks of degree ν. This implies that all synapses have the same strength g_c, but results will also apply to nonbinary Γ_c matrices as long as they are balanced.

The solution of Eq. (5) is generically unique, because only at a few discrete values of g_c (when it equals the inverse of an eigenvalue of Γ_c) will the system matrix be singular. Thus, generically, at most one equilibrium point can exist where all neurons are above synaptic threshold level. The solution will be valid only if $x_*^i > \phi^i$ for $i = 1, \ldots, N$. Let us suppose that this is the case and analyze the stability of this fixed point. The Jacobian of the system of Eqs. (3) can be separated into intrinsic and coupling parts as

$$J = \mathcal{F} + \mu g_c\Gamma_c \otimes K_c.$$

(6)

$\mathcal{F}$ is a $2N \times 2N$ block-diagonal matrix where each 2×2 block is

$$F^i = \begin{pmatrix} f'(x_*^i) & 1 \\ -\mu^i & 1 \end{pmatrix}.$$

(7)

We have abused notation making $f'(x) = \delta f(x, y)/\delta x$ and we suppose that all $x_*^i < 0$; that is, that they are in the non-

linear part of $f(x, y)$. The symbol $\otimes$ stands for the tensor or Kronecker product and K_c is the 2×2 synaptic coupling matrix

$$K_c = \begin{pmatrix} 0 & 0 \\ 1 & 0 \end{pmatrix}.$$

In the general case there is little more we can do; we need to diagonalize the Jacobian case by case and study its eigenvalues as a function of parameters. But when the network is homogeneous and balanced, the equilibrium state is also homogeneous, that is, $x_*^i = x_*$ for all i. We may explicitly obtain it from Eq. (5) as

$$x_* = \frac{-1 + \sigma - g_c\nu\phi}{1 - g_c\nu}.$$

(8)

Now every F^i is the same matrix F and the Jacobian can be compactly written

$$J = I_N \otimes F + \mu g_c\Gamma_c \otimes K_c,$$

(9)

where I_N is the $N \times N$ identity matrix. In this case we can diagonalize the Jacobian simply by diagonalizing Γ_c, and obtaining a block diagonal matrix with each block (2×2) given as

$$M_k = F + s_k\mu g_c K_c = \begin{bmatrix} f'(x_*) & 1 \\ \mu(-1 + g_c s_k) & 1 \end{bmatrix}$$

(10)

$$= \begin{bmatrix} \dfrac{\alpha(1 - g_c\nu)^2}{[2 - \sigma - (1 - \phi)g_c\nu]^2} & 1 \\ \mu(-1 + g_c s_k) & 1 \end{bmatrix},$$

(11)

where $k = 0, \ldots, N-1$ and s_k are the eigenvalues of Γ_c. For each eigenvalue of Γ_c we obtain a block M_k of the full Jacobian. The stability of the equilibrium solution requires that the eigenvalues of each M_k matrix have absolute value lower than 1. We thus obtain a function, the maximum absolute value of the eigenvalues of M_k, that, for given neuron parameters α, μ, and σ, and connectivity parameters g_c, ν, ϕ, and s_k, determines the stability of the network around the fixed point. This is called the master stability function [16] and is a powerful tool to separate the influence of the network topology on stability from that of the intrinsic neuron dynamics.

Observe that each M_k block produces two eigenvalues and eigenvectors of the Jacobian (9). Each eigenvector is tangent to an invariant manifold that, when the mode is dominant (i.e., when it is the only unstable mode or its exponential rate of growth is by far the highest) will define the evolution of the system. We will therefore need to calculate the dominant eigenvectors of the Jacobian to draw conclusions about network activity patterns. Fortunately, there is a direct relationship between eigenvectors of the Jacobian and of Γ_c. It is straightforward to prove that if $\mathbf{v}_k$ is the $(N \times 1)$ eigenvector of Γ_c with eigenvalue s_k, and if $\mathbf{w}_{k1,2}$ are the (2×1) eigenvectors of block M_k, then the eigenvectors of the Jacobian (9) corresponding to that block are $\mathbf{v}_k \otimes \mathbf{w}_{k1,2}$. This means that all the information about the behavior of each neuron in a mode is contained in $\mathbf{v}_k$, while the $\mathbf{w}_{k1,2}$ eigenvectors just
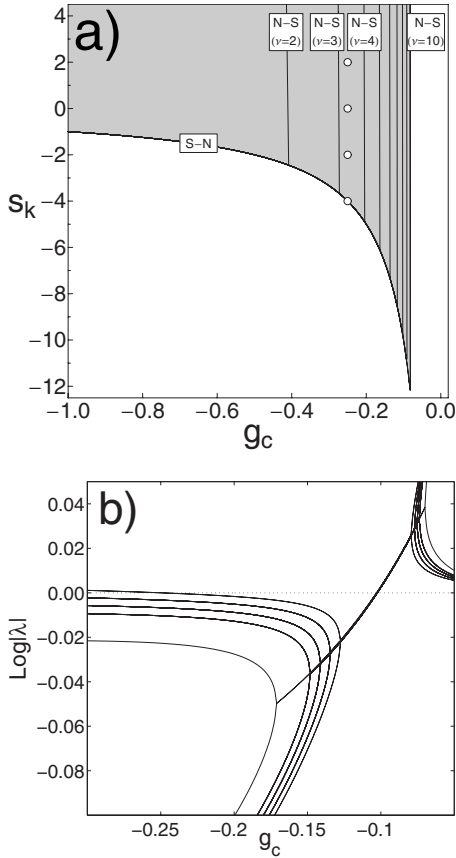
FIG. 4. (a) Master stability contours in the $g_c - s_k$ plane of the uniform fixed point for balanced symmetric networks of Rulkov neurons with different degrees ν. The boundaries marked *N-S* correspond to Neimark-Sacker bifurcations, while the boundary marked *S-N* corresponds to saddle-node bifurcations. Modes that fall inside the shaded area are stable. Circles represent graph eigenvalues of a 4×4 periodic lattice with 8-neighborhood, drawn at $g_c = -0.25$, precisely where one mode (corresponding to row or column activity) becomes unstable. (b) Natural logarithm of the absolute values of the eigenvalues of the Jacobian (9) for the periodic 4×4 lattice with 8-neighborhood around the uniform fixed point as a function of g_c. All modes gain stability near $g_c = -0.1$ through Neimark-Sacker bifurcations and become unstable for lower values of g_c (beginning at $g_c = -0.25$) through degenerate saddle-node bifurcations. Other parameters are $\alpha = 6$, $\mu = 0.001$, $\sigma = 0$, and $\phi = -2$.

provide proportionality constants for the fast and slow variables. We will thus describe the modes of the full system simply by looking at the components of the eigenvectors of Γ_c.

A. Stability analysis of symmetric networks

When the network is symmetric, as in the case of the examples presented in Sec. III, all the s_k are real. This allows a clear graphical representation of stability as a function of network topology and strength of inhibition. Contours in Fig. 4(a) represent, for different values of the degree ν of the network, the points in the g_c-s_k plane where the modulus of the maximum eigenvalue of M_k is 1. For a given symmetric network with balanced inhibition, we only need to place its

eigenvalues s_k on the chart and see at what value of g_c they cross the stability contour corresponding to its degree ν. These crossings correspond to bifurcations in the full system; we will see in Eqs. (12) and (13) that crossing the vertical contours corresponds to Neimark-Sacker bifurcations, while crossing the hyperbolic contour corresponds to saddle-node bifurcations. In the figure, the eigenvalues s_k of the 4×4 lattice with 8-neighborhood are represented at the value of g_c where the uniform silent state is about to lose stability. We can see there that the mode with eigenvalue $s_{1,2} = -4$, which has multiplicity 2, is responsible for the loss of stability. The corresponding eigenvectors are

$$\mathbf{v}_1 = (1, 0, 1, 0, 0, -1, 0, -1, 1, 0, 1, 0, 0, -1, 0, -1),$$

$$\mathbf{v}_2 = (0, 1, 0, 1, -1, 0, -1, 0, 0, 1, 0, 1, -1, 0, -1, 0).$$

Observe that $\mathbf{v}_1 + \mathbf{v}_2$ corresponds to row modes while $\mathbf{v}_1 - \mathbf{v}_2$ corresponds to column modes. Of course depending on initial conditions any linear combination $\beta_1 \mathbf{v}_1 + \beta_2 \mathbf{v}_2$ may be amplified, but in the end only the signs of the resulting vector elements matter to decide which neurons are drawn toward bursting and which toward silence. Thus only four patterns (even rows, odd rows, even columns, and odd columns) result when inhibition provokes the loss of stability. If inhibition is strong enough, other eigenvalues will also cross the stability boundary, but the rate of growth of the row and column modes will always be highest and almost every initial condition will end up with the row or column pattern.

Figure 4(b) represents the eigenvalues of the uniform equilibrium of the 4×4 lattice with an 8-neighborhood as a function of g_c; it can be seen as a superposition of horizontal cross sections of the master stability chart at the s_k values of the network. All modes gain stability at around $g_c = -0.103$ (corresponding with the almost vertical contour in the master chart) and lose it at different values of g_c, the first at $g_c = -0.250$ (these are the two $s_k = -4$ modes).

In the case of the regular random network of Fig. 3, the most negative eigenvalue is $s_k = -4.17$ and its eigenvector is

$$\mathbf{v}_k = (0.33, -0.05, 0.12, 0.37, 0.32, -0.09, 0.34, -0.29, -0.08,$$
$$-0.34, 0.20, 0.03, 0.07, -0.27, -0.17, -0.40).$$

Observe that the two groups of neurons of Fig. 3 correspond to eigenvector elements of the same sign. Neuron 12, which was inactive in both cases, has the smallest component; it is only weakly excited with this mode and the suprathreshold pattern of the network prevents it from bursting. One particularity is worth elaborating: The eigenvector components sum up to zero. This holds for any symmetric matrix with constant row sums because of orthogonality with respect to the all-ones eigenvector. This, and numerical exploration of symmetric random matrices, suggests that there are usually about the same number of negative and positive components in the dominant eigenvector of symmetric networks, and with strong enough inhibition neurons will split into two groups of similar size, one or the other being active depending on initial conditions.

The master stability chart in Fig. 4 is valid only for our particular choice of parameters α, μ, σ, and ϕ. We can overcome this shortcoming by using directly the explicit expression (11) to find bifurcation points. For a Neimark-Sacker bifurcation, the necessary condition $\lambda_1 \bar{\lambda}_2 = 1$ (with λ_1, λ_2 the eigenvalues of M_k) together with $\mu \ll 1$ yields

$$f'(x_*) \approx 1 \Rightarrow g_c \approx \frac{-2 + \sigma + \sqrt{\alpha}}{\nu(\sqrt{\alpha} - 1 + \phi)}. \tag{12}$$

The condition $f'(x_*) \approx 1$ is the same as in an isolated Rulkov neuron; it is the Neimark-Sacker bifurcation that happens when σ is lowered to the point where the slow nullcline crosses the stable branch of the fast nullcline and stops the bursting. Here the effective σ is lowered by the inhibitory connections with immediate neighbors. Observe that the condition is independent of s_k; thus all modes gain stability with increasing $|g_c|$ at almost the same time (the differences due to the neglected term of the order of μ). In the master stability chart the bifurcation corresponds to the almost vertical boundary lines; note the inverse proportionality between ν and g_c as predicted in Eq. (12).

The necessary condition (12) does not guarantee that the eigenvalues will be complex. For this, it is also necessary that $g_c s_k < 1$. Thus, the boundary segments given by Eq. (12) end at the point where $g_c s_k = 1$. These points form a second boundary, defined by a saddle-node bifurcation. Indeed, forcing Eq. (11) to have $\lambda_1 = 1$ we obtain the saddle-node bifurcation condition

$$g_c s_k = 1. \tag{13}$$

This condition is independent of neuron parameters and of ν; it corresponds to the branch of hyperbola shared by all contours in Fig. 4. While the Neimark-Sacker bifurcations could be explained from the point of view of an isolated neuron in terms of the effective change in the excitation σ due to the influence of neighboring neurons (thus their dependence on ν), in the saddle-node bifurcations all the neurons in the network take part (thus their dependence on the s_k). They have no natural isolated-neuron equivalent: It would consist of a change in the sign of μ. It is at this bifurcation that the higher order properties of the connectivity graph show up, and the modes are cleanly separated, making the one with the most negative s_k dominant. This allows us to predict easily at which inhibition strength the network will begin to burst with the pattern of the dominant mode. It is worth noting that the bifurcation only involves the unique fixed point of the network above synaptic threshold; it takes place without the collision and disappearance of a pair of equilibrium points. This degeneracy is due to the neutral stability of the slow variable.

We can now prove the generality of the sequence shown in Fig. 4(b), where, as g_c decreases from zero towards negative values, first all modes undergo a gain of stability through a Neimark-Sacker bifurcation, and later some of them lose that stability through a saddle-node bifurcation. The Neimark-Sacker bifurcation will take place if condition (12) is met with $g_c s_k < 1$ for all s_k. That is, if $s_{k,\min}$ is the most negative s_k, we must have
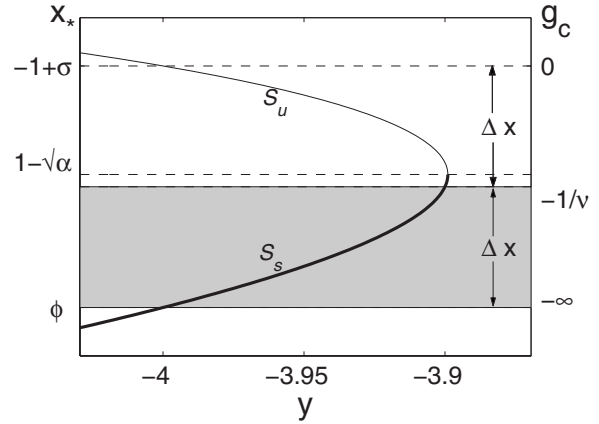
FIG. 5. Phase plane of the Rulkov model with the position of the homogeneous equilibrium level x_* (left axis) corresponding to values of g_c (right axis). The $g_c = -1/\nu$ level is exactly midway between $x_* = -1 + \sigma$ and $x_* = \phi$. Since condition (15) is met, it is below the Neimark-Sacker level $x_* \approx 1 - \sqrt{\alpha}$. Thus, growing inhibition first drives the network into silence and only afterwards is the mode with the most negative eigenvalue excited, at the point in the shadowed region corresponding to $g_c = 1/s_{k,\min}$. Parameters of the Rulkov neuron are $\alpha = 6$ and $\mu = 0.001$.

$$\frac{s_{k,\min}}{\nu} > \frac{\sqrt{\alpha} - 1 + \phi}{-2 + \sigma + \sqrt{\alpha}}. \tag{14}$$

But we know that the eigenvalues of a regular graph have modulus less or equal to the degree of the graph [17]. Thus $s_{k,\min}/\nu \geq -1$ and we may ensure that Eq. (14) is satisfied for any regular symmetric network if

$$1 - \sqrt{\alpha} > \frac{1}{2}[(-1 + \sigma) + \phi]. \tag{15}$$

As long as Eq. (15) is met, all modes will gain stability at the value of g_c given by Eq. (12). Only at a more negative g_c value (indeed, at $g_c < -1/\nu$, since $s_{k,\min} \geq -\nu$) will the mode corresponding to the lowest s_k meet condition (13), losing stability through the saddle-node bifurcation. As g_c decreases further, all modes with $s_k < 0$ will become unstable one after another, at $g_c = 1/s_k$. On the other hand, since all symmetric regular networks have at least one eigenvalue $s_k \leq -1$ [17], the first loss of stability must necessarily happen at $g_c \geq -1$.

The meaning of the constraint (15) is best understood by following the position of the fixed point x_*, given by Eq. (8), in the phase plane of the Rulkov model, as g_c goes from 0 to $-\infty$. This is shown in Fig. 5. When $g_c = 0$, $x_* = -1 + \sigma$, the level of the slow nullcline of an isolated neuron. As g_c decreases, x_* shifts down and, when it arrives at $x_* = 1 - \sqrt{\alpha}$ (the vertex of the fast nullcline), all modes become stable through a Neimark-Sacker bifurcation. As we have explained in the previous paragraph, this stability can only be lost for $g_c \leq -1/\nu$, which corresponds to $x_* \leq \frac{1}{2}[(-1 + \sigma) + \phi]$. Thus, if the condition (15) is met, only after all modes have become stable will the mode with the lowest s_k lose stability through a saddle-node bifurcation. An interval of g_c exists, between

the value given by Eq. (12) and $g_c = 1/s_{k,\min}$, where the uniform fixed point of the system, and thus the regime of silence, is locally stable.

It is worth noting that the stability of the uniform fixed point does not preclude sustained activity in the network. In the 4×4 periodic lattice example, the uniform fixed point is stable between $g_c = -0.103$ and $g_c = -0.250$, but it is globally attracting only between $g_c = -0.162$ and $g_c = -0.250$. We shall discuss the relationship between local and global dynamics further in Sec. V.

We wish to finish this subsection with a remark on the secondary pattern found in the 4×4 periodic lattice of Fig. 2 when inhibition is $g_c \leq -0.5$. It can be explained as a bifurcation around the nonuniform fixed points such as the one shown in Fig. 2 for $g_c = -0.49$; there are four of these corresponding to row and column distributions of neurons above and below synaptic threshold. The master stability technique cannot be used for these nonuniform equilibria, but we may calculate, as we did in Fig. 4(b), the eigenvalues of the system around them. The result appears in Fig. 6(a). It looks like the superposition of the eigenvalue charts of two regular networks. Indeed, in the row or column pattern, half of the neurons are below the synaptic threshold and thus have no functional outgoing connections; they behave like isolated neurons with a low effective σ due to their six active neighbors. On the other hand the neurons over the threshold behave as two separate 4×1 rings, i.e., regular networks of degree $\nu = 2$, with minimum eigenvalue $s_k = -2$. Thus according to Eqs. (12) and (13) we expect them to become silent somewhere below $g_c = -0.408$ and begin firing again at $g_c \leq -0.5$ with an alternating pattern. This is in fact what happens, and our explanation of Fig. 2 is now complete.

B. Stability analysis of general balanced networks

When the network is not symmetric, eigenvalues of the connectivity matrix will generally be complex. We cannot use a g_c-s_k planar chart as in Fig. 4 to gain insight, but we still can draw conclusions for matrix M_k in Eq. (11). The Neimark-Sacker bifurcation that brings about the stability of the fixed point, given by Eq. (12), was independent of s_k in the $\mu \ll 1$ approximation, and continues to be when s_k is complex. On the other hand, the condition in Eq. (13) for the destabilizing saddle-node bifurcation cannot be fulfilled with a complex $s_k = a_k + ib_k$; indeed a $\lambda = 1$ eigenvalue is impossible. We may instead search for an eigenvalue $\lambda_k = e^{i\omega_k}$ with $\omega_k \ll 1$ and obtain another Neimark-Sacker bifurcation satisfying

$$g_c = 1/a_k, \quad \omega_k = \mu \frac{g_c b_k}{1 - f'(x_*)}. \quad (16)$$

The conjugate eigenvalues that cross the unit circle are $\lambda_{k1,k2} = e^{\pm i\omega_k}$, and they come to two different M_{k1} and M_{k2} blocks of the Jacobian (9) with $s_{k1,k2} = a_k \pm ib_k$. As we see, $\mu \ll 1$ ensures $\omega_k \ll 1$ as long as $f'(x_*)$ is not close to 1, which is the condition for the other, s_k-independent, Neimark-Sacker bifurcation of Eq. (12). Thus in asymmetric networks, instead of the saddle-node bifurcations at $g_c = 1/s_k$, we have
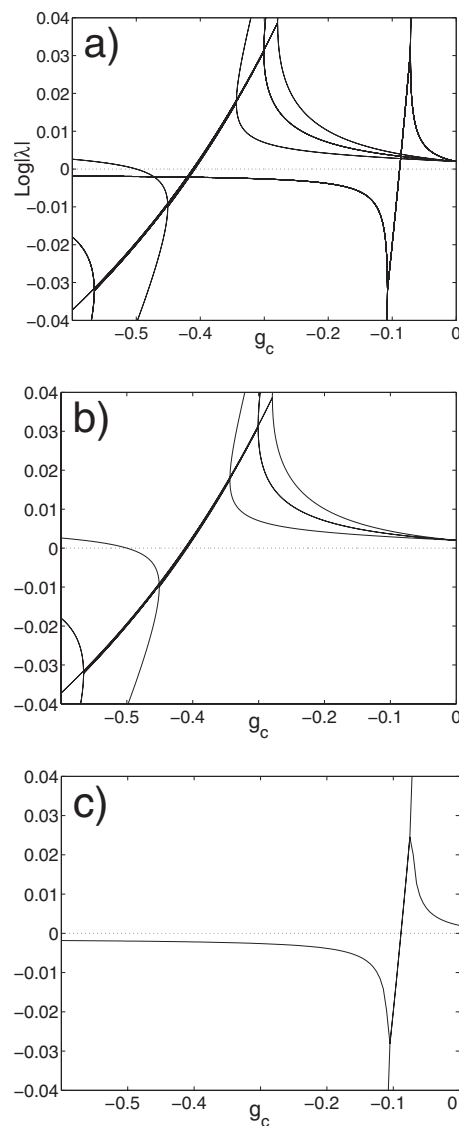
FIG. 6. As a function of g_c, logarithmic representation of the eigenvalues of the Jacobian (9) for (a) the 4×4 lattice with 8-neighborhood around the fixed point in the row or column configuration, (b) a 4×1 ring around the homogeneous equilibrium, and (c) an isolated neuron with a value of σ that accounts for the inhibition received from six active neighboring neurons. The superposition of (b) twice and (c) eight times yields (a). Other parameters are $\alpha = 6$, $\mu = 0.001$, $\sigma = 0$ [except in (c)], and $\phi = -2$.

Neimark-Sacker bifurcations at $g_c = 1/a_k$ with a very low frequency $\omega_k \ll 1$.

We can therefore expect the same picture as in symmetric networks, with all neurons firing at low inhibition strengths, then stable silence at intermediate strengths, and finally bursting in part of the network when inhibition goes beyond $g_c = 1/a_{k,\min}$. When the network is random, the value of $a_{k,\min}$ is easy to predict thanks to the circular law [18], which states that the eigenvalues of a random matrix of i.i.d. samples of a random variable X with zero mean and variance σ_X^2 tend to be uniformly distributed in a circle of radius $r = \sigma_X \sqrt{N}$ when the size $N \times N$ of the matrix grows to infinity. In our balanced networks, since row sums are constant and the diago-
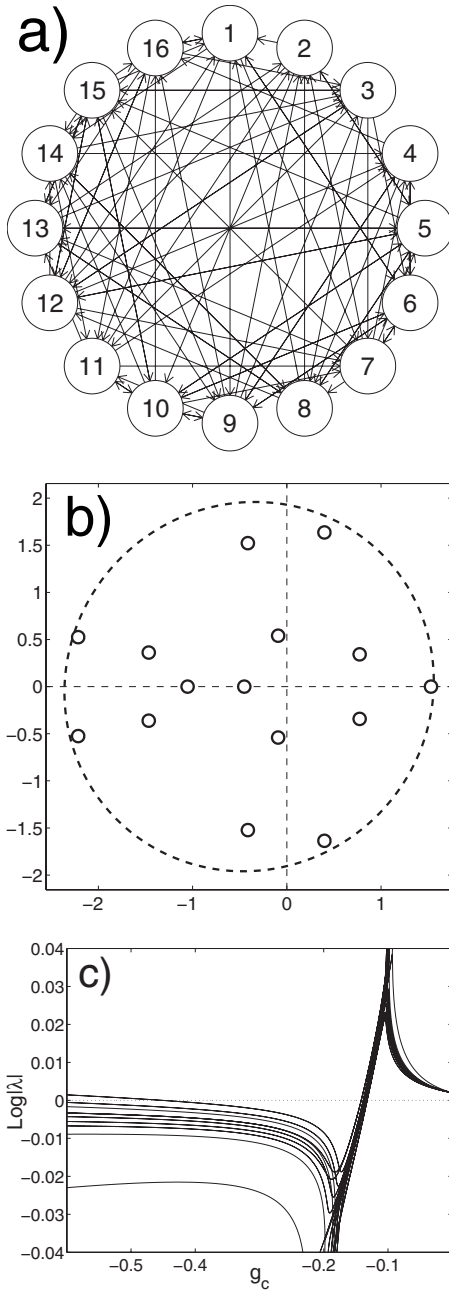
FIG. 7. (a) An asymmetric balanced network of $N=16$ neurons with $\nu=6$ input connections in each neuron. (b) Eigenvalues of the connectivity matrix of the network in the complex plane. The dashed circumference is the expected area of distribution of the eigenvalues according to the circle law. The eigenvalue $s_0=6$ is not shown. (c) Eigenvalues of the Jacobian (9) around the homogeneous equilibrium point x_* as a function of g_c. Other parameters are $\alpha=6$, $\mu=0.001$, $\sigma=0$, and $\phi=-2$.

nal elements are zero, the independence hypothesis is not fully satisfied, but this only produces one positive real eigenvalue $s_0=\nu$ and displaces the center of the circle to $c=-\nu/(N-1)$. The law works well even for small matrix sizes and we may use it to approximate the minimum real part of the s_k as $a_{k,\min}\approx-r+c$. The distribution of eigenvalues in the circle is slightly affected by the lack of indepen-

dence [19] and suffers from the smallness of the system, but this has little relevance for our results because we are interested mainly in the dominant mode.

Figure 7(a) shows an asymmetric random balanced network of $N=16$ neurons with input degree $\nu=6$. All synapses have the same strength. Thus, except for the constant sum constraint, the nondiagonal elements of the connectivity matrix Γ_c may be considered samples of i.i.d. Bernoulli random variables of mean $p=\nu/(N-1)$. The circle law expects the eigenvalues of such matrix to be distributed in the circle of center $(-p,0)$ and radius

$$r = \frac{\sqrt{\nu(N-1-\nu)N}}{N-1}.$$

Therefore we expect the eigenvalue with the most negative real part to be no further than $-p-r=-2.36$. The actual eigenvalues are depicted in Fig. 7(b), with the leftmost conjugate pair at $a_{k,\min}=-2.21$. With such a small network, the discrepancy is not surprising. In Fig. 7(c) the corresponding loss of stability can be seen at $g_c\approx-1/2.21\approx-0.452$. Observe also the Neimark-Sacker bifurcations around the value predicted in Eq. (12) for $\nu=6$, namely $g_c\approx-0.14$.

In order to know the pattern of activity that sets in when stability is lost we look at the eigenvectors of the dominant mode. If, as in the example of Fig. 7, the cause of instability is a pair of complex conjugate eigenvalues of Γ_c giving rise to the Neimark-Sacker bifurcation of a pair of complex conjugate boxes M_k of the Jacobian (9), the mode will consist of a pair of conjugate eigenvectors producing oscillations.

Figure 8 shows the time evolution of the network of Fig. 7 for two values of g_c: One barely past the loss of stability and the other with slightly stronger inhibition. Oscillations just above the bifurcation are subthreshold, almost linear and stable (the bifurcation is supercritical). They are slow, their frequency correctly given by w_k in Eq. (16). Amplitude and phase of the oscillations is encoded in the modulus and angle of the complex components of any of the two eigenvectors; these are depicted in the left part of the figure. As inhibition grows the oscillations also grow and we should expect the neurons corresponding to the components of maximum modulus to be the first to burst. In the example, neurons 13 and 5 have the highest amplitudes but neuron 5 does not burst, while smaller amplitude neurons 10, 12, and (sometimes) 8 do. This is a clustering effect. See in the figure that neurons 10 and 12 have high amplitudes and phases similar to neuron 13; when the latter bursts, it boosts neurons with a similar phase to do the same, and draws neurons in the opposite part of the cycle toward negative voltages (note the notches in the trace of neurons 5, 7, 14, 15, and 16). This lowers the subsequent maximum of their oscillation and prevents them from firing. If due to initial conditions neuron 5 fires first, it may carry neurons 7 and 16 with it, but their combination is weaker than that of neurons 13, 12, and 10 and unable to prevent their bursts. Interestingly, although all synapses are inhibitory, some neurons have indirect excitatory effects on each other due to mode formation.

When inhibition goes further beyond the instability threshold, oscillations grow in all neurons and different pat-
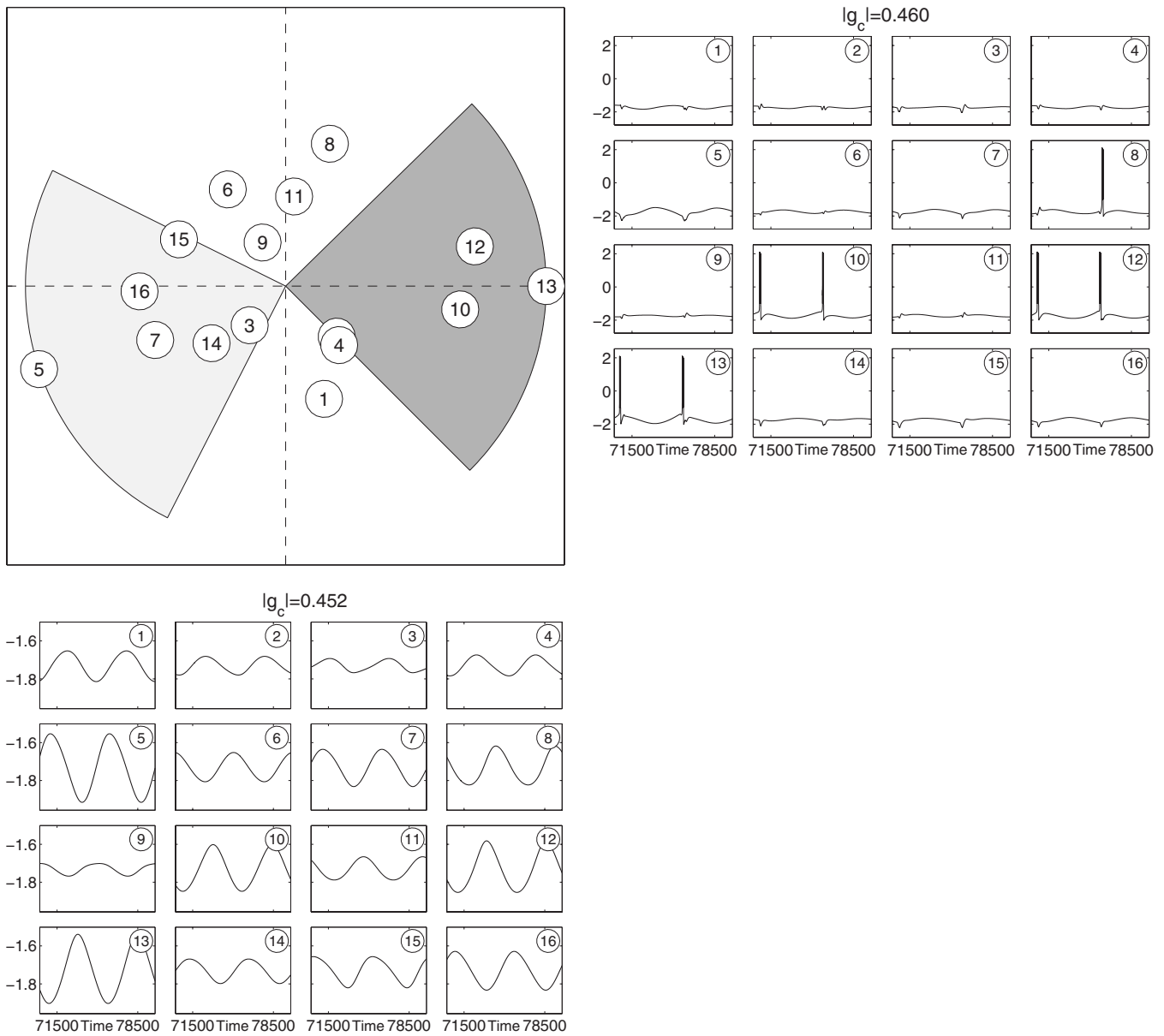
FIG. 8. Top Left: Complex plane with the components of one of the two conjugate eigenvectors of the dominant mode of the network in Fig. 7. The dark and light gray sectors span 90° around components 13 and 5, respectively, to help see groups of neurons tending to burst together. Bottom: Activity in the network barely past instability. Note that amplitudes and phases correspond with the eigenvector component diagram. Right: Activity for slightly stronger inhibition.

terns emerge. Figure 9 shows raster plots of network activity for three values of g_c. The first corresponds to the same value shown in Fig. 8, right. Neurons 13 fires first, triggering bursts in neurons 12, 10, sometimes followed by neuron 8, and inhibiting the opposite phase cluster. The sequence of eigenvector component angles would predict neuron 10 to fire first, but it has lower amplitude and cannot do it by itself; it is instead carried along, when already past the maximum of its oscillation, by the burst of neuron 13. When $g_c=-0.5$, the cluster of neuron 13 is joined sometimes by lower amplitude neurons 1, 2 and 4 (note that in Fig. 8 the component of neuron 2 is hidden behind that of neuron 4) while in the opposite part of the cycle neuron 5 fires, sometimes together with high-amplitude, similar-phase neurons 7 and 16. With

very strong inhibition $g_c=-0.8$ most of the neurons burst forming a very characteristic pattern, where we may discern again the opposing neuron-13 and neuron-5 clusters. Observe how neuron 8 bursts in the transition between the two, as corresponds to its phase in Fig. 8, and also that now neuron 10 does burst before neurons 13 and 12. Neurons with high amplitude in the diagram of Fig. 8 burst several times in each cycle, because their slow-wave oscillation remains above bursting threshold long enough to fit more than one burst (burst duration is determined mostly by the intrinsic parameters of the neuron). Bursts affect the subthreshold period, and with $g_c=-0.8$ we can see that the period is significantly lengthened compared to the linear prediction of Eq. (16).
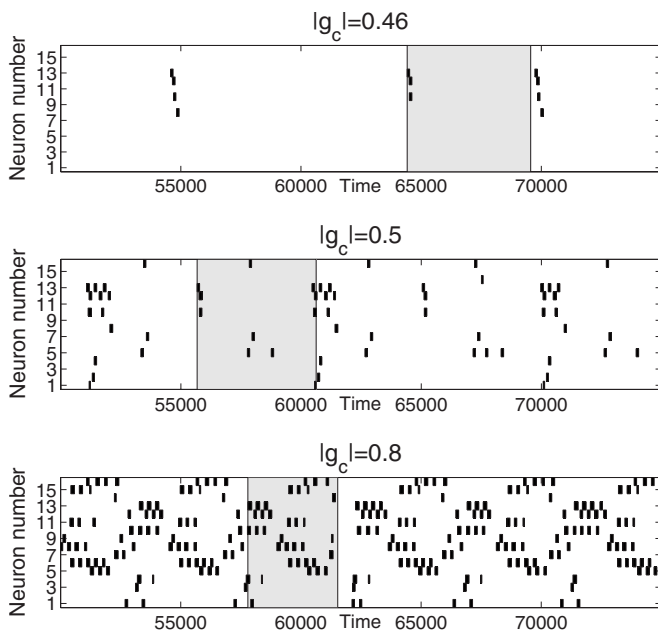
FIG. 9. Raster plots of the activity in the network of Fig. 7 for different strengths of inhibition. Black patches mark bursting periods of each neuron. Gray areas mark the length of the period predicted by the ω_k in Eq. (16).

V. DISCUSSION

We have seen how the symmetry, balance and most importantly the spectral properties of the topology determine the activity patterns observed in networks of bursting inhibitory neurons. Linear analysis around the fixed point of the system has allowed us, by simply looking at the eigenvalues and dominant eigenvectors of the network graph, to predict the pattern of bursts as a function of the strength of inhibition. Since the fixed point is unstable for those values of g_c
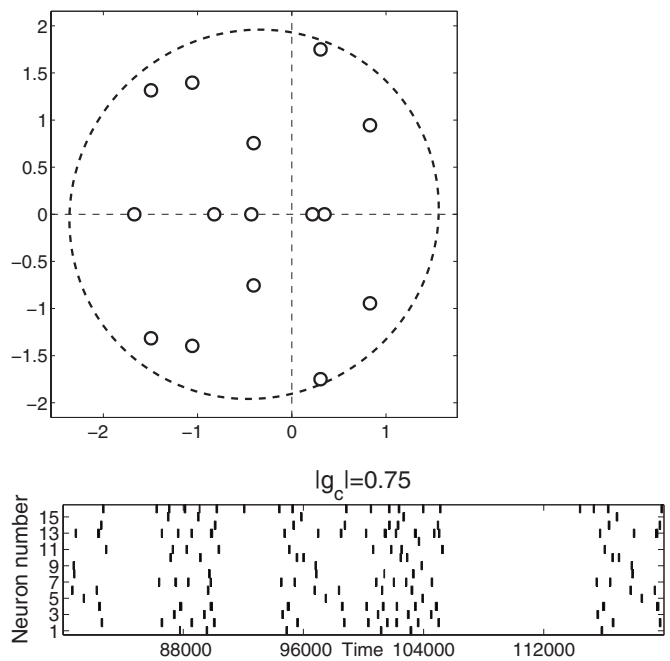
FIG. 10. Eigenvalues of the connectivity matrix of an asymmetric balanced network of $N=16$ neurons with input degree $\nu=6$, and raster plot of its activity. The modes corresponding to the leftmost real eigenvalue and the leftmost pair of conjugate eigenvalues are both unstable, and this results in a complex pattern.

that produce activity, the validity of this technique depends on reinjection, i.e., the system must repeatedly pass near the fixed point for its modes to dominate the dynamics. The intrinsic bursting dynamics of the neurons ensures indeed that the subthreshold region of the state space is visited for almost all initial conditions. Besides this, the dominant mode must have noticeably faster growth than the other modes; otherwise a mixture of modes sets in and the prediction of
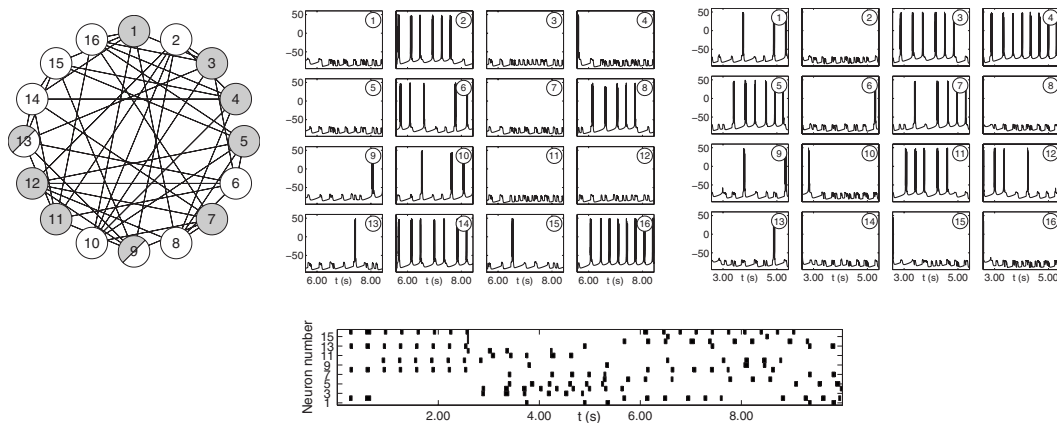
FIG. 11. Patterns of activity in the symmetric network of Fig. 3 using Hodgkin-Huxley type models of thalamic reticular neurons connected through $GABA_A$ and $GABA_B$ synapses, instead of Rulkov neurons. Above, left: The structure of the network. White and gray neurons represent the two groups that seem to alternate in the resulting pattern; note that they are the same as in Fig. 3, except for neurons 9 and 13, which are here weakly active with both groups, and neuron 12, which fires with the group that corresponds to the sign of its eigenvector component. Above, center and right: Two different moments along a 10 s simulation, showing the two groups of active neurons. Below: Raster plot of the 10 s simulation, showing the alternation of the two groups of active neurons. The description of the neuron and synapse model can be found in [22]. Synaptic conductances are $g_{GABA_A}=g_{GABA_B}=0.1$ μS. A constant external current $I=0.1$ μA/cm^2 is injected in the soma of all neurons to place them in the bursting regime.

the pattern is not obvious. Figure 10 shows the eigenvalues and activity of an asymmetric network with two dominant modes (one real and one complex); the result is a rich pattern whose relationship with the eigenvectors of the two modes is not evident. In large networks, when the eigenvalues of the connectivity matrix are densely packed, mode mixture is unavoidable and statistical approaches should be used [20].

As we have seen in the previous section, asymmetric networks with a complex dominant mode have a rhythmic behavior marked by the slow subthreshold oscillations over which the bursts ride. Besides, with strong enough inhibition, almost all neurons participate in the activity at different phases of the slow cycle. This contrasts sharply with symmetric networks (or asymmetric with a real dominant mode) where the only rhythm present is the fast intrinsic bursting frequency, and where (when only one mode is dominant) two mutually exclusive groups form and only one of them is active, depending on initial conditions. But there is another level of pattern formation in symmetric networks that we have not analyzed; namely, the sequence of bursts inside the active group. Note, for example, in Fig. 2 that for $g_c = -0.40$ bursts inside the active rows alternate between neighbors. In the random network of Fig. 3, the sequence of bursts is persistent and robust against initial conditions although this cannot be appreciated in the figure.

These burst sequence patterns, in fact, appear in the weak inhibition regime (when all neurons are active) in both symmetric and asymmetric networks; they appear in Fig. 2 for $|g_c| < 0.20$. If we see them also in the strong inhibition regime of symmetric networks, it is because there a new, less dense, effective network has formed containing only the active neurons (remember that in the case of the lattice this has allowed us to explain the secondary patterns for $g_c < -0.50$). This effective network is again in a weak inhibition regime, and bursts follow in it a certain sequence that depends on g_c.

At any rate, the burst sequence in the weak inhibition regime cannot be directly derived from the linear properties around the fixed point. For example, the eigenvalues of the Jacobian (9) for the 4×4 lattice, shown in Fig. 4(b), give, for low strength of inhibition, no hint about the values of g_c at which the different bursting sequences set in. Indeed, these sequences can be found in exactly the same order when the synaptic threshold is placed at a high voltage ($\phi = 0$, for example), which makes the fixed point nonexistent [due to the Heaviside function in Eq. (4)].

This brings us to one important limitation of our study, namely the low synaptic threshold. Patterns of synchronization are very sensitive to the synaptic threshold [21]. Normally, the threshold for synaptic interaction is set above spike initiation, because spikes, and not subthreshold dynamics, are responsible for the postsynaptic potentials. If we wish to carry over our analysis to a model with high synaptic threshold we may substitute the study of stability of the fixed point, which will no longer exist, by that of a synchronous bursting trajectory; but in that case we lack a reinjection mechanism that ensures that the dynamics near that trajectory are dominant.

Our choice of model and coupling has allowed us to establish the link between the spectral properties of the adjacency matrix and the dynamics of the network. We wish to
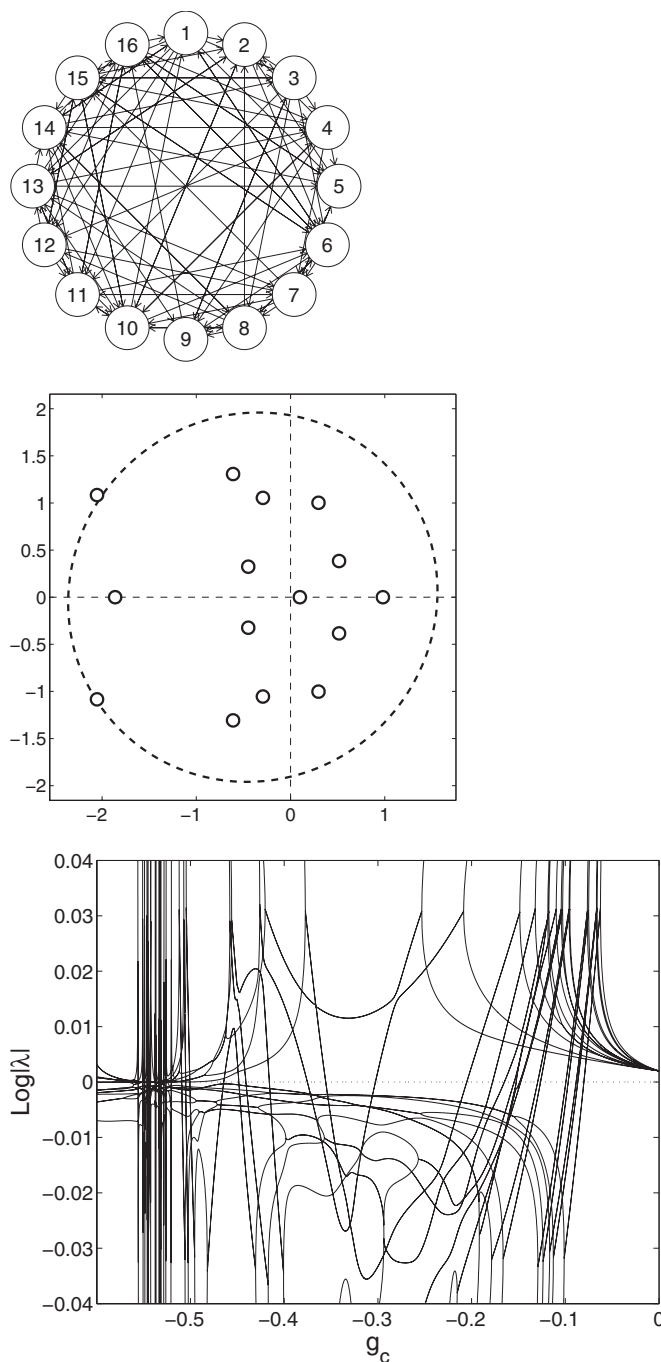
FIG. 12. Top: Nonbalanced network of $N=16$ neurons. The input degree to each neuron has been randomly chosen between 4 and 8. Center: Eigenvalues of the connectivity matrix in the complex plane. The real eigenvalue $s_0 = 5.97$ is not shown. Bottom: Eigenvalues of the Jacobian (6) around the equilibrium point $\mathbf{x}_*$ given by Eq. (4) as a function of g_c. Other parameters are $\alpha=6$, $\mu=0.001$, $\sigma=0$, and $\phi=-2$.

note that this link is also apparent in biologically plausible models. In Fig. 11 we have kept the same connectivity graph of Fig. 3, but we have replaced the Rulkov neurons and direct coupling with thalamic reticular neurons connected through $GABA_A$ and $GABA_B$ synapses [22]. The same two complementary groups of neurons, corresponding to different signs in the components of the eigenvector of the domi-

nant eigenvalue of the adjacency matrix, show up in the simulation, although here we find them alternating in an apparently random fashion along the same run. The alternation is suppressed if either the fast $GABA_A$ or the slow $GABA_B$ synapses are eliminated, hinting at a complex interplay between their time constants. Stronger synapses also fix one of the two groups. More complex patterns, similar to those found in the weak inhibition regime of the Rulkov networks, arise from weaker synapses and different time constants.

This example shows that even in some cases that are not immediately amenable to master stability function decomposition, the spectrum of the adjacency matrix dominates the dynamics. To determine why this is so and, in the cases where it is not, what peculiarities of the connectivity graph are reflected in the pattern of activity, is open to research. Two restrictions of our study are certainly, in all cases, fundamental: The homogeneity and balance conditions. They ensure that spatial inhomogeneities can only arise from topological properties of the graph. In particular, in our study, they were required for the fixed point to be homogeneous, so that mode structure was exclusively due to the network topology embodied in Γ_c in Eq. (9). If the network is not balanced or not homogeneous, the equilibrium levels x_*^i are different for the different neurons, and thus another level of structure is added to the network in top of the topology of connections. As a result, the Jacobian (6) can no longer be diagonalized with the same matrix as Γ_c, and there is no direct relationship between the spectrum of Γ_c and that of the system. The difficulty is compounded by the fact that x_* enters the stability equations through the nonlinearity $f(x)$. In Fig. 12 we see that, while the eigenvalues of Γ_c for a nonbalanced network do not differ wildly from those of a balanced network, the eigenvalues of the system around the equilibrium point do show a very complex dependence on g_c. We can still, for a given level of inhibition, analyze the dominant mode of the whole system, but cannot draw conclusions about it by simply looking at the spectrum of the connection graph. If the imbalance or the inhomogeneity are small we may approximate the perturbation of the Jacobian by a linear term dependent on Γ_c, and perhaps this would allow an extension of the master stability method. The feasibility and usefulness of this approach is left for future work.

A minor point for further discussion arises from the type of Neimark-Sacker bifurcation of our model. The linear analysis we have performed of the oscillatory modes in asymmetric networks depends on the corresponding Neimark-Sacker bifurcation being supercritical and thus giving rise to a small stable limit cycle. The Rulkov model, with its neutral slow variable, favors the supercritical behavior [13]. It would be interesting to investigate the phenomenon in a subcritical model.

We have used small networks to easily visualize the results. They hold equally for somewhat larger random networks (in the order of tens or a hundred neurons), as long as single mode dominance prevails. This scale is appropriate for most central pattern generators. But if the network under study has a highly modular, nonrandom structure, the technique will carry over to much larger sizes thanks to the associated nonuniform spectral distribution (as in the lattice example). This is important because many prototypical neural systems, including neocortex, cerebellar cortex and hippocampus, are highly modular and structured [23]. Besides, recent research on the structure of the cortex reveals that a small number of strong connections may constitute the driving core of cortical dynamics [24]. Thus medium sized systems with nonrandom topology can reveal important features of extended ensembles of neurons. As our knowledge of the structure of the nervous system deepens, rough models based on spotty statistical evidence are superseded by more detailed and structured networks. The approach followed in this paper can provide valuable insight into their dynamics.

ACKNOWLEDGMENTS

[1] H. D. I. Abarbanel, M. I. Rabinovich, A. Selverston, M. V. Bazhenov, R. Huerta, M. M. Suschchik, and L. L. Rubchinskii, Phys. Usp. **39**, 337 (1996).

[2] M. Steriade and D. A. McCormick, Science **262**, 679 (1993).

[3] W. Schultz, J. Neurophysiol. **80**, 1 (1998).

[4] J. Aguirre, E. Mosekilde, and M. A. F. Sanjuán, Phys. Rev. E **69**, 041910 (2004).

[5] G. N. Orlovsky, T. G. Deliagina, and S. Grillner, *Neuronal Control of Locomotion: From Mollusc to Man* (Oxford University Press, New York, 1999).

[6] E. Marder and D. Bucher, Curr. Biol. **11**, R986 (2001).

[7] J. M. Casado, B. Ibarz, and M. A. F. Sanjuán, Mod. Phys. Lett. B **18**, 1347 (2004).

[8] J. M. Casado, Phys. Rev. Lett. **91**, 208102 (2003).

[9] I. V. Belykh, E. de Lange, and M. Hasler, Phys. Rev. Lett. **94**, 188101 (2005).

[10] N. F. Rulkov, I. Timofeev, and M. Bazhenov, J. Comput. Neurosci. **17**, 203 (2004).

[11] G. Tanaka, B. Ibarz, M. A. F. Sanjuán, and K. Aihara, Chaos **16**, 013113 (2006).

[12] N. F. Rulkov, Phys. Rev. Lett. **86**, 183 (2001).

[13] B. Ibarz, G. Tanaka, M. A. F. Sanjuán, and K. Aihara, Phys. Rev. E **75**, 041902 (2007).

[14] N. F. Rulkov, Phys. Rev. E **65**, 041922 (2002).

[15] C. van Vreeswijk and H. Sompolinsky, Science **274**, 1724 (1996).

[16] L. M. Pecora and T. L. Carroll, Phys. Rev. Lett. **80**, 2109 (1998).

[17] D. M. Cvetkovic, M. Doob, and H. Sachs, *Spectra of Graphs. Theory and Applications*, Pure and Applied Mathematics (Aca-

demic Press, New York, 1979).

[18] V. L. Girko, Theor. Probab. Appl. **29**, 694 (1984).

[19] J. Stäring, B. Mehlig, Y. V. Fyodorov, and J. M. Luck, Phys. Rev. E **67**, 047101 (2003).

[20] D. J. Amit and N. Brunel, Cereb. Cortex **7**, 237 (1997).

[21] F. K. Skinner, N. Kopell, and E. Marder, J. Comput. Neurosci. **1**, 69 (1994).

[22] M. Bazhenov, I. Timofeev, M. Steriade, and T. J. Sejnowski, J. Neurophysiol. **79**, 2730 (1998).

[23] S. Grillner, H. Markram, E. de Schutter, G. Silberberg, and F. E. LeBeau, Trends Neurosci. **28**, 525 (2005).

[24] S. Song, P. J. Sjöström, M. Reigl, S. Nelson, and D. B. Chklovskii, PLoS Biol. **3**, e68 (2005).